Scientific Reports

https://doi.org/10.1038/s41598-026-60621-8

Article in Press

Enhanced borohydride electrocatalysis through electronic coupling of PtNi nanomaterials and reduced graphene oxide

Received: 18 April 2026

Accepted: 29 June 2026

Published online: 02 July 2026

Cite this article as: Halvacı E., Bayat R., Seyrankaya A. *et al.* Enhanced borohydride electrocatalysis through electronic coupling of PtNi nanomaterials and reduced graphene oxide. *Sci Rep* (2026). https://doi.org/10.1038/s41598-026-60621-8

Ebru Halvacı, Ramazan Bayat, Abdullah Seyrankaya, Mustafa Ucar & Fatih Sen

We are providing an unedited version of this manuscript to give early access to its findings. Before final publication, the manuscript will undergo further editing. Please note there may be errors present which affect the content, and all legal disclaimers apply.

If this paper is publishing under a Transparent Peer Review model then Peer Review reports will publish with the final article.

ARTICLE IN PRESS

© The Author(s) 2026. **Open Access** This article is licensed under a Creative Commons Attribution-NonCommercial-NoDerivatives 4.0 International License, which permits any non-commercial use, sharing, distribution and reproduction in any medium or format, as long as you give appropriate credit to the original author(s) and the source, provide a link to the Creative Commons licence, and indicate if you modified the licensed material. You do not have permission under this licence to share adapted material derived from this article or parts of it. The images or other third party material in this article are included in the article's Creative Commons licence, unless indicated otherwise in a credit line to the material. If material is not included in the article's Creative Commons licence and your intended use is not permitted by statutory regulation or exceeds the permitted use, you will need to obtain permission directly from the copyright holder. To view a copy of this licence, visit http://creativecommons.org/licenses/by-nc-nd/4.0/.

ARTICLE IN PRESS

Enhanced Borohydride Electrocatalysis through Electronic Coupling of PtNi Nanomaterials and Reduced Graphene Oxide

Ebru Halvacı[1], Ramazan Bayat[1], Abdullah Seyrankaya[2], Mustafa Ucar[3], Fatih Sen[1]*

[1]Sen Research Group, Biochemistry Department, Dumlupinar University, Evliya Celebi Campus, 43100, Kutahya, Türkiye.

[2]Mining Engineering Department, Faculty of Engineering, Dokuz Eylul University, Tınaztepe Campus, 35210 Izmir, Türkiye.

[3]Chemistry Department, Faculty of Arts and Science, Afyon Kocatepe University, 03200, Afyon, Türkiye.

Corresponding Author: fatihsen1980@gmail.com

ARTICLE IN PRESS

Abstract

In this study, a PtNi nanocomposite supported on reduced graphene oxide (rGO) was synthesized via a chemical reduction method, and its electrocatalytic performance for the electrochemical oxidation of sodium borohydride ($NaBH_4$) was investigated. The structural and morphological properties of the synthesized PtNi@rGO nanocomposite were characterized in detail using FTIR, XRD, TEM, and SEM-EDX analyses. The characterization results demonstrated that the PtNi alloy nanoparticles were successfully immobilized on the rGO surface and were homogeneously distributed in the 20–50 nm size range. Electrochemical performance studies were conducted using the cyclic voltammetry method in a solution containing 1 M NaOH and 0.1 M $NaBH_4$. The results revealed that the PtNi@rGO electrocatalyst achieved a maximum current density of 19.57 mA cm^{-2}, while under the same conditions, the PtNi and Pt electrodes exhibited values of 17.19 and 6.53 mA cm^{-2}, respectively. Furthermore, the determined initial potential of 0.13 V for PtNi@rGO indicated a faster reaction kinetics compared to the PtNi (0.17 V) and Pt (0.22 V) electrodes. Analyses conducted at different scan rates

ARTICLE IN PRESS

demonstrated that the reaction proceeded in a kinetically controlled manner and that the rGO support significantly improved charge transfer processes. Long-term stability tests have demonstrated that the developed nanocomposite maintains its electrocatalytic performance. The results indicate that the PtNi@rGO nanocomposite is a stable and promising electrocatalyst with high activity for hydrogen production via the electrooxidation of $NaBH_4$.

Keywords: PtNi alloy, reduced graphene oxide, PtNi@rGO nanocomposite, electrooxidation of sodium borohydride, hydrogen production, electrocatalysis.

1. Introduction

Carbon-based energy production has a direct impact on climate change due to high CO_2 emissions and environmental pollutants; this situation has made the need for low-carbon energy carriers a critical area of research [1], [2], [3]. In this context, hydrogen is recognized as one of the clean energy vectors of the future due to its high gravimetric energy density and the fact that it produces only water as a combustion byproduct [4], [5]. However, since hydrogen does not occur in a free state in nature, it is necessary to develop alternative hydrogen carriers for production and storage processes. In this context, borohydride ($NaBH_4$) has become one of the chemical hydrogen sources that has been extensively studied in recent years due to its high hydrogen content and controlled release capacity [6], [7]. The electrochemical oxidation of $NaBH_4$ offers an important route for hydrogen production at low temperatures; however, the efficiency of this reaction depends largely on the catalytic activity at the electrode surface [8], [9]. While the literature indicates that the oxidation of $NaBH_4$ should theoretically occur via eight electron transfers, in practical systems the reaction is predominantly controlled by complex surface processes [10], [11]. In particular, the formation of intermediate borane species, surface adsorption, and simultaneous hydrogen evolution have been reported as key factors

ARTICLE IN PRESS

limiting the actual electron transfer efficiency. Consequently, the design of electrocatalysts that provide high activity and stability has become a critical area of research determining the performance of this reaction [12], [13], [14]. In addition, the precise control of electronic band structures enables the enhancement of catalytic activity and selectivity. In particular, hydrogen extraction from hydrogen carrier compounds, such as $NaBH_4$, can be significantly optimized with nanomaterials in terms of low energy requirements and controlled hydrogen release [15], [16]. Thus, the advantages offered by nanomaterials are not limited to the laboratory scale, but also guide large-scale applications [17], [18], [19], [20], [21]. Nanocatalysts are attracting attention as advanced materials that provide high efficiency and stability in $NaBH_4$-based hydrogen production processes. Due to $NaBH_4$'s high hydrogen capacity (10.8% by weight H_2) and controlled hydrogen release potential, it is considered an ideal hydrogen carrier for renewable energy technologies [22], [23], [24]. However, an effective nanocatalyst is required for it to be hydrolyzed efficiently and in a controlled manner [25], [26], [27], [28]. In recent years, intensive research has been conducted not only on Pt-based systems but also on various mono- and bimetallic electrocatalysts containing Pd, Ni, Co, and Cu for the electrochemical oxidation of borohydride [29]. It has been reported in the literature that Pd-based systems exhibit high initial activity, particularly in terms of the hydrogen adsorption–desorption equilibrium but show limitations regarding long-term stability and surface passivation. Similarly, while bimetallic structures containing Ni and Co can improve BOR kinetics due to cost advantages and electronic structure modification, they cannot provide sufficient electron transfer efficiency and active site stability when used alone [30], [31]. While Cu-based catalysts offer lower-cost alternatives, they lag behind Pt-based systems in terms of intrinsic catalytic activity. In this context, Pt-containing bimetallic systems, such as Pt–Ni, offer a more balanced catalytic behavior by optimizing the surface binding energies of intermediate species through the tuning of the d-band center [32], [33].

ARTICLE IN PRESS

However, most studies in the literature focus either solely on the alloy effect or solely on the carbon support effect, and the joint evaluation of metal–metal and metal–carbon interactions remain limited [34]. In particular, the synergistic effect of hybrid structures formed by two-dimensional conductive materials, such as reduced graphene oxide (rGO), on the electron transfer kinetics of these different metallic systems has not been sufficiently and systematically demonstrated.

Within the scope of this study, a PtNi@rGO nanocomposite electrocatalyst was successfully prepared and its catalytic behaviour in the electrochemical oxidation reaction of $NaBH_4$ was systematically evaluated. Structural and electrochemical analyses indicate that the electronic structure modification associated with Ni doping at the Pt–Ni alloy sites rearranges the Pt d-band centre, and that this optimises the surface binding energies of intermediate species, thereby accelerating the reaction kinetics. Furthermore, the high electrical conductivity of rGO reduces charge transfer resistance by forming a continuous electron transport network, thereby enhancing the effective utilisation of active sites. As a result of this synergistic interaction, PtNi@rGO emerges as a high-performance electrocatalytic platform for $NaBH_4$ oxidation, exhibiting not only enhanced catalytic activity but also long-term electrochemical stability and accelerated electron transfer kinetics.

2. Materials and Methods

2.1. Chemicals

Platinum (II) chloride ($PtCl_2$), nickel (II) acetate tetrahydrate ($Ni(OCOCH_3)_2{\cdot}4H_2O$), graphite, sodium nitrate ($NaNO_3$), sulfuric acid (H_2SO_4), potassium permanganate ($KMnO_4$), hydrogen peroxide (H_2O_2), sodium borohydride ($NaBH_4$), sodium hydroxide (NaOH) chemicals are used in the study without any purification.

2.2. Reduced Graphene Oxide Synthesis

ARTICLE IN PRESS

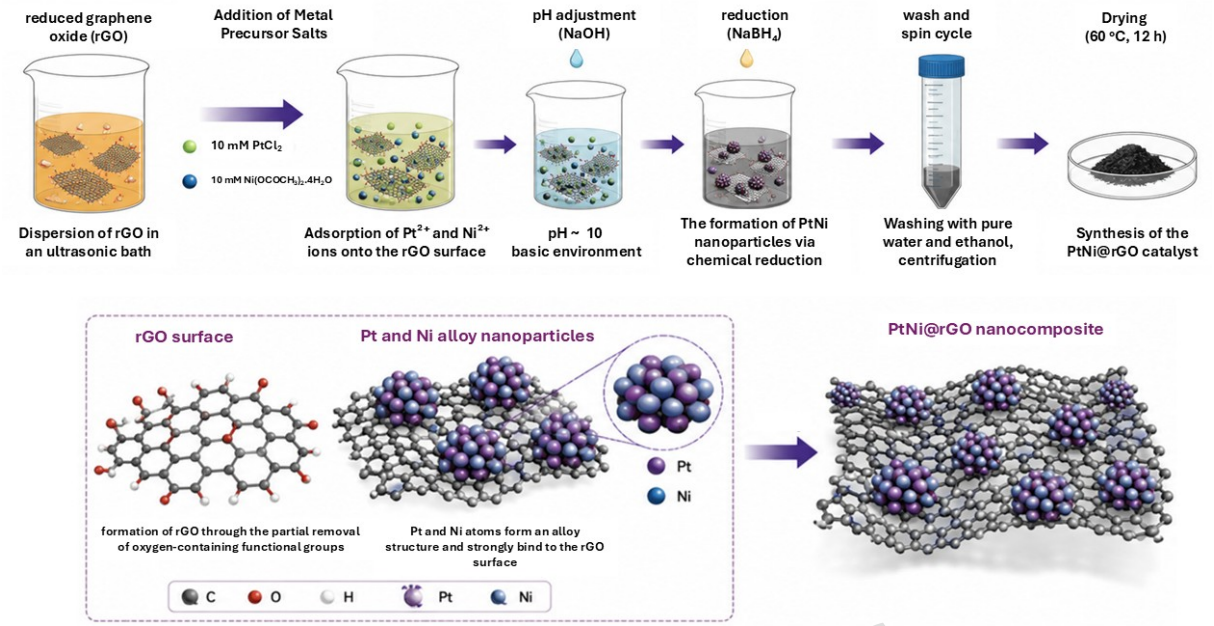
To form reduced graphene oxide (rGO), graphene oxide (GO) is first synthesized. In this context, 2 g of graphite and 2 g of $NaNO_3$ are added to 90 ml of H_2SO_4 and stirred at 5 °C for 4 hours. Then, 12 g of $KMnO_4$ is added, and the reaction is continued for about 2 hours, maintaining the temperature at an average of 5 °C. After 2 hours, 250 ml of pure water is added to the reaction medium at 35-40 °C, and stirring is continued for another hour. After the process, 40 ml of H_2O_2 is added to the reaction medium for another 2 hours. Finally, the resulting mixture is centrifuged until completely clear, and the resulting material is washed several times with 10% HCl and deionized water (dH_2O). The resulting material is dried at 60 °C [35], [36] and after drying, the resulting material is calcined at 350 °C for 10 min to form the rGO structure [37].

2.3. PtNi@rGO Synthesis

PtNi@rGO synthesis is carried out using the $NaBH_4$ chemical reduction method, which is a fast and inexpensive method. In this context, first, 16 mg of rGO is dissolved in 20 mL of dH_2O, then 10 mM $PtCl_2$ and 10 mM $Ni(OCOCH_3)_2.4H_2O$ are added, and the mixture is stirred for 30 minutes in a magnetic stirrer. After stirring, 50 mg of $NaBH_4$ is added and stirred for 90 min at room temperature. Finally, the resulting particles are collected at 4000 rpm for 15 min and washed several times with dH_2O. The resulting mixture is dried overnight at 50 °C in an oven. Similar procedures are performed for PtNi and Pt nanocatalysts. In addition, the synthesis route of the PtNi@rGO nanocomposite is shown schematically in Scheme 1.

ARTICLE IN PRESS

ARTICLE IN PRESS



Scheme 1. A schematic illustration of the formation of the PtNi@rGO nanocomposite through the chemical reduction of Pt and Ni precursors on the rGO surface.

2.4. Characterization of PtNi@rGO

The synthesized PtNi@rGO was characterized using various techniques. Among these, XRD crystal structure analysis was performed using a Rigaku miniflex model device. In addition, a Hitachi Regulus 8230 model field emission scanning electron microscope (FE-SEM) was used to analyze the three-dimensional structure of the material. Finally, the atomic-level structure and elemental composition of the material were analyzed using a transmission electron microscope (TEM), model JEOL JEM-1220.

2.5. Electrochemical Studies

Studies on the electrooxidation of $NaBH_4$ are being conducted using the obtained PtNi@rGO, PtNi, and Pt catalysts. Electrochemical measurements are performed on a Gamry Interface 1000 Potentiostat device using a triple electrode system consisting of an Ag/AgCl reference electrode, a platinum sheet counter electrode, and a glassy carbon electrode. For surface

ARTICLE IN PRESS

modification of the working electrode, 3 mg of PtNi@rGO, PtNi, and Pt nanoparticles are taken and dispersed separately in 1 ml of Nafion using a sonicator. Then, 10 mg of the obtained electrocatalyst ink is dropped onto the glassy electrode surface and dried at 25 °C for 30 min. Electrochemical studies are performed in a 1 M NaOH medium containing 0.1 M $NaBH_4$ [38].

3. Results and Discussion

3.1. Characterization

The FTIR spectrum shown in Figure 1a, obtained to elucidate the chemical structure of the PtNi@rGO nanocomposite, revealed the presence of strong interactions among the components within the material structure. The sharp peak at 1719 cm^{-1} (C=O stretching) and the band at 1578 cm^{-1} (C=C stretching) observed in the spectrum of the reduced graphene oxide (rGO) phase confirm the presence of the graphene skeleton. they also indicate that oxygen-containing groups in the form of carboxylic acids are partially preserved even after the conversion from GO to rGO [39]. This supports the existence of critical nucleation sites for the attachment of PtNi nanoparticles to the surface. In the composite spectrum, the proximity and slight shift between the peaks at 1050 cm^{-1} (C-O stretching) belonging to the oxygen-containing functional groups of rGO and 1020 cm^{-1} in PtNi@rGO, indicates a strong coordinative or electronic interaction between PtNi nanoparticles and the alkoxy/epoxy groups on the rGO surface. Furthermore, the broad band at 3410 cm^{-1} (-OH stretching) in the composite material is evidence of the hydrophilic character and remaining hydroxyl groups on the material surface. Overall, the FTIR results confirm that the oxygen-containing groups on rGO act as stabilizers and binding agents for PtNi nanoparticles, preventing the aggregation of the composite and confirming its high surface area structure [40].

In this study, distinct diffraction peaks were observed at angles of 24.75°, 40.15°, 46.66°, 67.77°, 81.78°, and 86.06° in the XRD pattern of the PtNi@rGO nanocomposite shown in Figure 1b. The characteristic diffraction

ARTICLE IN PRESS

peaks obtained from the XRD analysis indicate the presence of the (111), (200), (220), (311), and (222) crystal planes of the PtNi alloy phase, along with the (002) plane of the rGO support. The d-spacing values calculated using the Bragg equation were determined to be approximately 2.24 Å (111), 1.96 Å (200), 1.38 Å (220), 1.18 Å (311), and 1.13 Å (222), respectively. These values are consistent with results reported in the literature for PtNi-based alloy nanostructures and confirm the successful formation of the alloy [41], [42], [43]. Additionally, the diffraction peak appearing at 24.75° in the XRD pattern of the PtNi@rGO nanocomposite represents the (002) plane corresponding to the carbon layers in the rGO structure. In addition, the crystal structure of the PtNi@rGO nanocomposite shown in Figure 1c was evaluated in detail using the Scherrer and Williamson–Hall (W–H) methods. The fact that the average crystallite size calculated using the Scherrer equation is of the same order of magnitude as the values obtained from the W–H analysis suggests the nanocrystalline nature of the synthesized structure. The slope value obtained from the W–H analysis indicates that lattice deformations and internal strain effects arising during alloy formation may be present in the structure. However, the limited linearity of the fit suggests that the peak broadening is not solely strain-induced; it is also attributed to nanoscale effects, crystal defects, and structural irregularities associated with alloy formation. Similar behaviors have been reported in the literature for PtNi-based alloy nanoparticles, and it has been noted that such structural defects can positively influence electrocatalytic performance by increasing the density of active sites [45]-[48].

ARTICLE IN PRESS

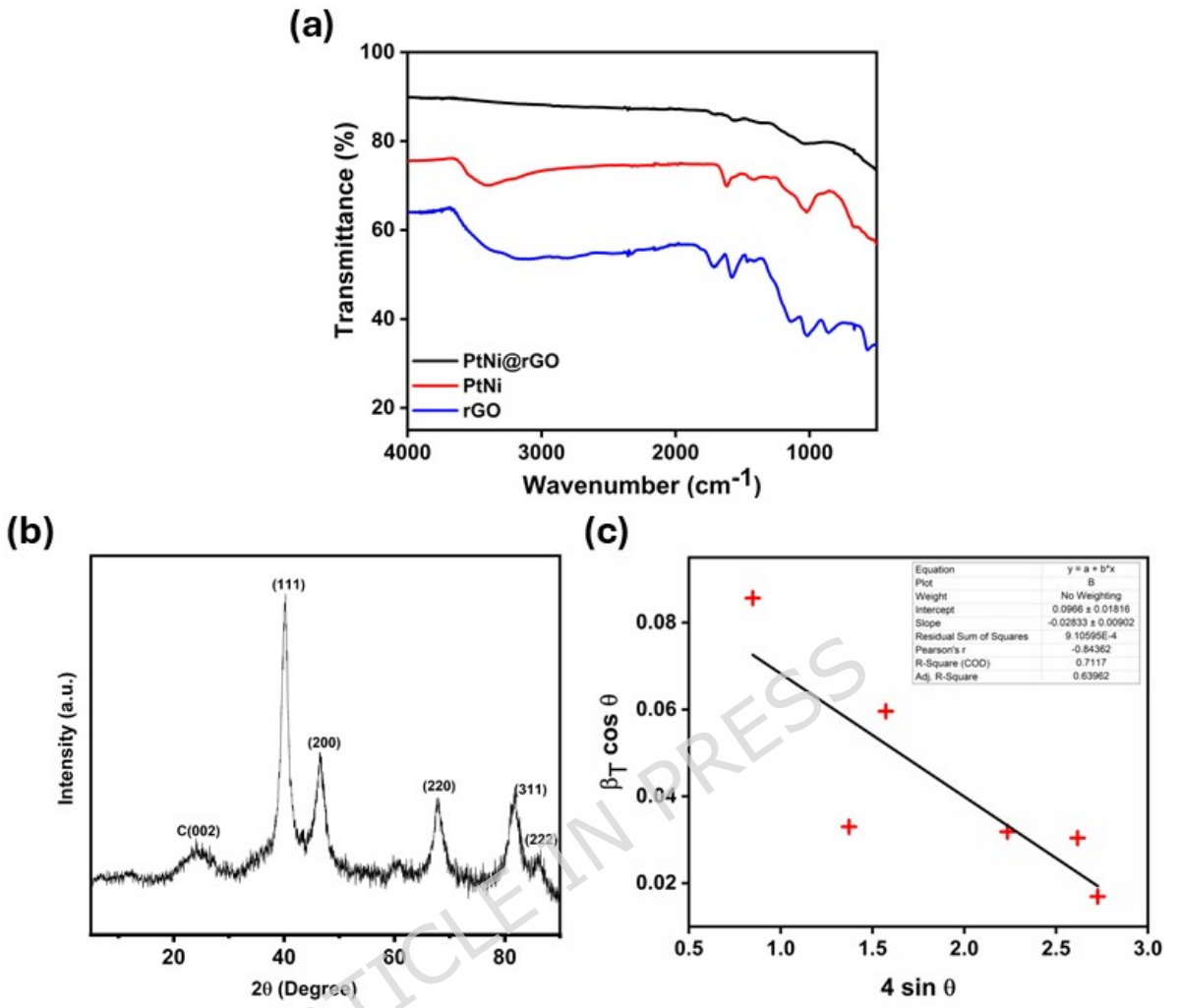


Figure 1. (a) FTIR spectrum, **(b)** XRD diffraction pattern and **(c)** Williamson Hall plots from the data of X-ray diffraction, a plot of β_T cosθ and sinθ is created of PtNi@rGO.

The general TEM image presented in Figure 2a and 2b reveals the morphological characteristics of the synthesized PtNi@rGO nanocomposite. In the obtained image, dark-toned metallic nanoparticles are observed to be homogeneously distributed on the thin, semi-transparent structure of the reduced graphene oxide (rGO) layer. These dark areas correspond to PtNi composite nanoparticles with high electron density. These results are consistent with previously reported PtNi@rGO systems in the literature [48]. The strong adsorption of nanoparticles onto the rGO surface indicates that

ARTICLE IN PRESS

the high surface area and functional groups of reduced graphene oxide support the nucleation of metal nanoparticles. This creates a synergistic effect, particularly in electrocatalytic applications, by facilitating charge transfer. Furthermore, Figure 2c and 2d show that some nanoparticles tend to cluster in small amounts at the edge regions, indicating the influence of local solution concentrations and surface energies during the growth process [49]. TEM images reveal that nanoparticles in the 20–50 nm range are uniformly distributed on the rGO surface. When evaluated together with the XRD results, this morphological structure suggests the successful formation of the PtNi alloy phase and the effective distribution of the nanoparticles on the rGO support. Furthermore, the consistency between the distinct crystal planes observed in XRD and the nanostructural distribution identified in TEM analyses supports the structural integrity of the synthesized PtNi@rGO nanocomposite.

ARTICLE IN PRESS

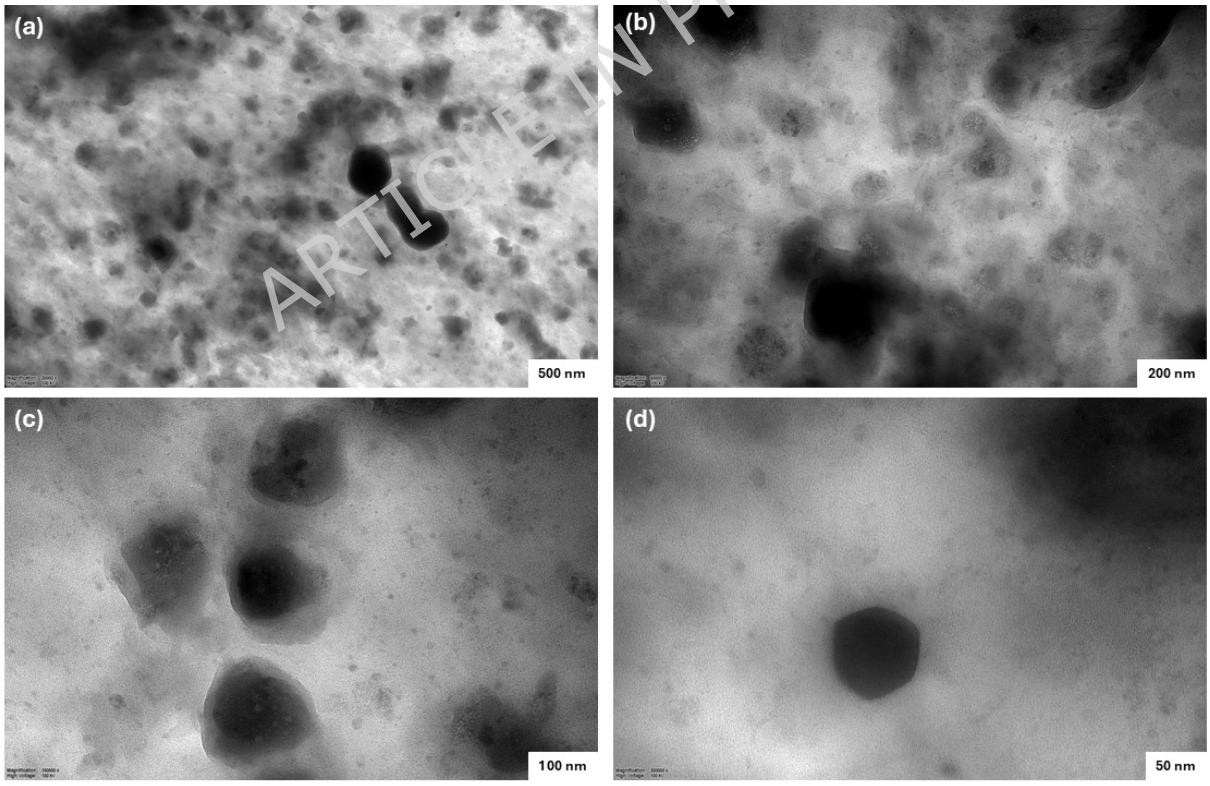


Figure 2. TEM images of the PtNi@rGO nanocomposite at **(a)** 500 nm, **(b)** 200 nm, **(c)** 100 nm, and **(d)** 50 nm magnification.

ARTICLE IN PRESS

The SEM images presented in Figure 3 (a-c) show the surface morphology and microstructural integrity of the synthesized PtNi@rGO nanocomposite. The images clearly show the rGO layers, which are characterized by a high surface area. This type of morphology indicates the structure of graphene oxide enriched with functional groups. This structure, observed in similar rGO-based structures, provides a surface suitable for the homogeneous dispersion of metal nanoparticles [50], [51]. The SEM images indicate that the PtNi@rGO nanocomposite possesses a porous and layered surface morphology. It is believed that the PtNi nanoparticles, which are homogeneously distributed on the rGO support, contribute to the formation of more accessible active sites by limiting excessive agglomeration on the surface. In particular, the alloy structure formed by Pt and Ni supports a more balanced distribution of nanoparticles on the surface, thereby creating a suitable surface architecture for electrocatalytic reactions. SEM-EDS analyses in Figure 3d revealed the sample's elemental composition by weight as 61.9% C, 32.8% O, 4.5% Ni, and 0.7% Pt. The carbon and oxygen contents are consistent with the structural character of the rGO support, and the detection of Ni and Pt elements suggests that the PtNi alloy has been successfully loaded onto the rGO surface [52]. The elemental mapping results shown in Figure 3e indicate that the Pt and Ni nanoparticles are uniformly distributed on the rGO support. Furthermore, the distribution of C and O elements shown in Figure 3f confirms that the graphene-based support structure has been successfully preserved. Such a structure increases the active surface area at the electrode-electrolyte interface and facilitates ion diffusion. In particular, the use of a PtNi alloy in combination with rGO provides a synergistic contribution to electron transport and reduces costs by lowering the metal load. This indicates that the synthesis conditions are under control and that the nanocomposite structure can possess high mechanical stability. The homogeneous distribution of PtNi nanoparticles on rGO serves as further evidence supporting the metal's chemical or electrochemical interaction with rGO.

ARTICLE IN PRESS

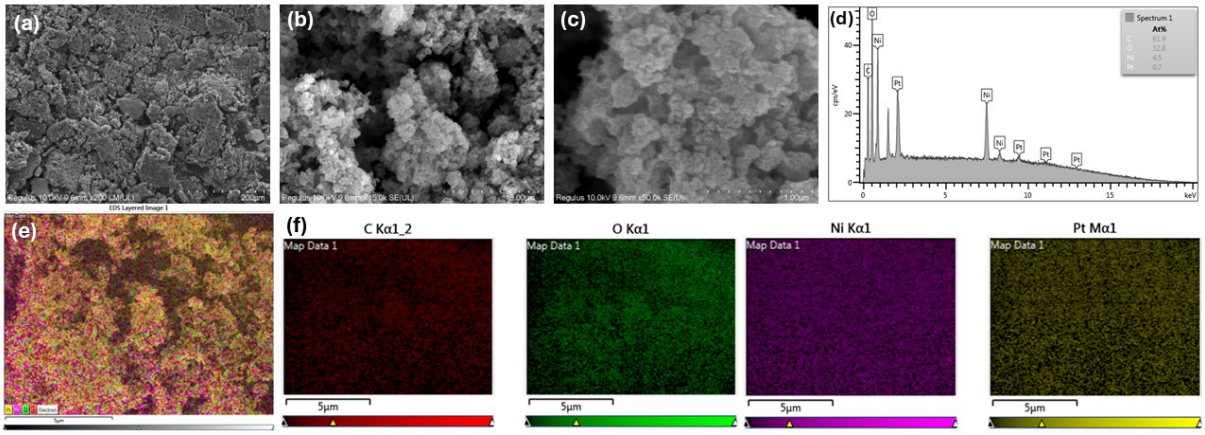


Figure 3. FE-SEM images of the PtNi@rGO nanocomposite: (a) 200 µm, (b) 3 µm, and (c) 1 µm magnifications; (d) EDS spectrum; (e) elemental mapping image; and (f) distribution maps for the elements Pt, Ni, C, and O.

The homogeneous distribution of PtNi nanoparticles on the rGO surface, as observed in TEM images, enables more efficient utilization of the active catalytic sites. Furthermore, the porous and layered morphology identified in SEM analyses increases the contact area between the electrolyte and the catalyst surface, facilitating easier access of reactive species to the active sites. When considered in conjunction with rGO's two-dimensional structure, which provides high conductivity, these morphological features contribute to the acceleration of electron transfer processes and a reduction in charge transport resistance. Consequently, the high current density and low onset potential observed in the PtNi@rGO electrocatalyst stem not only from the catalytic effect of the PtNi alloy but also from the advantages provided by the homogeneous nanoparticle distribution and the porous surface architecture.

ARTICLE IN PRESS

3.2. Electrochemical Measurements

After completing the XRD, SEM, and TEM analyses of the relevant material, the formation of 8 electrons in an alkaline environment as a result of the anodic reaction of NaBH4 is shown in equation 1 [53].

Anode: $NaBH_4^- + 8\ OH \rightarrow NaBO_2^- + 6\ H_2O + 8\ e^-$ (E_0 = -1.24 RHE) (Eq. 1)

ARTICLE IN PRESS

The electrochemical decomposition of $NaBH_4$, similar to NaOH, results in the formation of sodium metaborate ($NaBO_2^-$) and water along with 8 electrons [53], [54], [55].

Figure 4a, 4b, and 4c, respectively, present the CV results of PtNi@rGO, PtNi, and Pt electrocatalysts in a 1 M NaOH solution containing 0.1 M $NaBH_4$. Anodic peaks observed at all electrodes represent the electrochemical oxidation of borohydride ions, while peaks occurring in the cathodic region are associated with the reduction of surface-formed oxide species. Significant differences were observed between the electrodes, with the PtNi@rGO catalyst exhibiting both higher anodic current density and lower oxidation onset potential. PtNi@rGO reached a maximum current density of 19.57 mA cm^{-2}, while the same values were determined as 17.19 and 6.53 mA cm^{-2} for PtNi and Pt, respectively. Furthermore, the reduction of the oxidation onset potential to 0.13 V for PtNi@rGO indicates that the reaction occurs at a lower overpotential compared to PtNi (0.17 V) and Pt (0.22 V) systems. This observed improvement can be attributed to the modification of the electronic structure of the Pt surface as a result of the electronic interaction between Pt and Ni. Ni doping optimizes the adsorption/desorption balance of reaction intermediates by altering the d-band center of Pt, thus accelerating the borohydride oxidation kinetics. Additionally, rGO support reduces nanoparticle agglomeration, enabling more efficient utilization of active sites, and lowers electron transfer resistance due to its high electrical conductivity. Therefore, the synergistic effect created by the PtNi alloy effect and the conductive network structure of rGO can be considered the fundamental reason for the superior electrocatalytic performance of the PtNi@rGO electrode.

ARTICLE IN PRESS

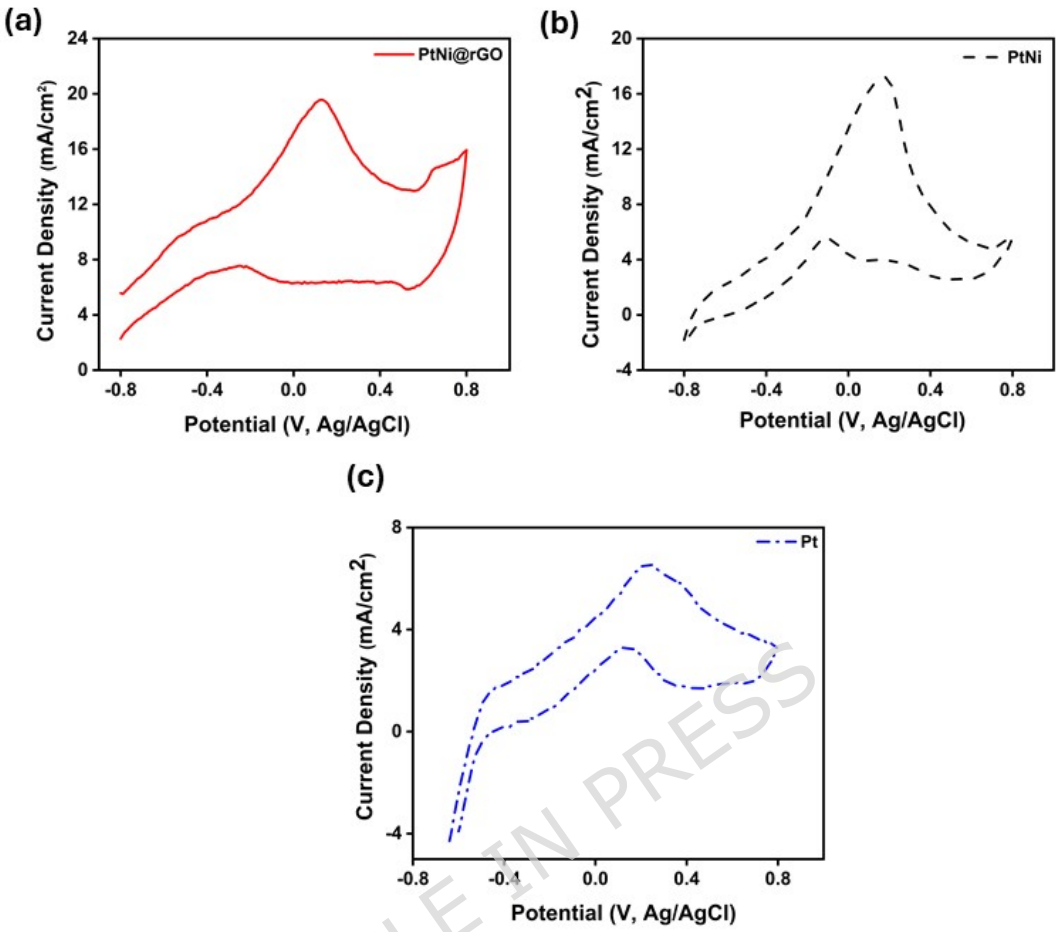


Figure 4. CV graphs of PtNi@rGO (a), PtNi (b), and Pt (c) nanoparticles in a 1 M NaOH solution containing 0.1 M $NaBH_4$.

Figure 5 shows a comparative evaluation of the maximum current density and oxidation initiation potentials of PtNi@rGO, PtNi, and Pt electrocatalysts. The PtNi@rGO catalyst exhibited both the highest current density and the lowest initiation potential, demonstrating more advantageous electrocatalytic behavior compared to the other electrodes. The increase in current density indicates that more active centers on the electrode surface participate in the reaction, resulting in faster borohydride oxidation. Conversely, the decrease in initiation potential shows that the reaction can be initiated with a lower energy requirement, improving charge transfer kinetics. In particular, the fact that PtNi@rGO produces approximately three times higher current

ARTICLE IN PRESS

density than the Pt electrode and exhibits a more negatively shifted initiation potential clearly indicates that alloy formation and rGO support together enhance catalytic activity. The high current density and low onset potential exhibited by the PtNi@rGO electrode are consistent with many Pt and Pt-based bimetallic electrocatalysts reported in the literature, and also parallel previous studies showing that the Pt–Ni alloy effect and carbon-supported conductive network structure improve boron kinetics [30], [56].

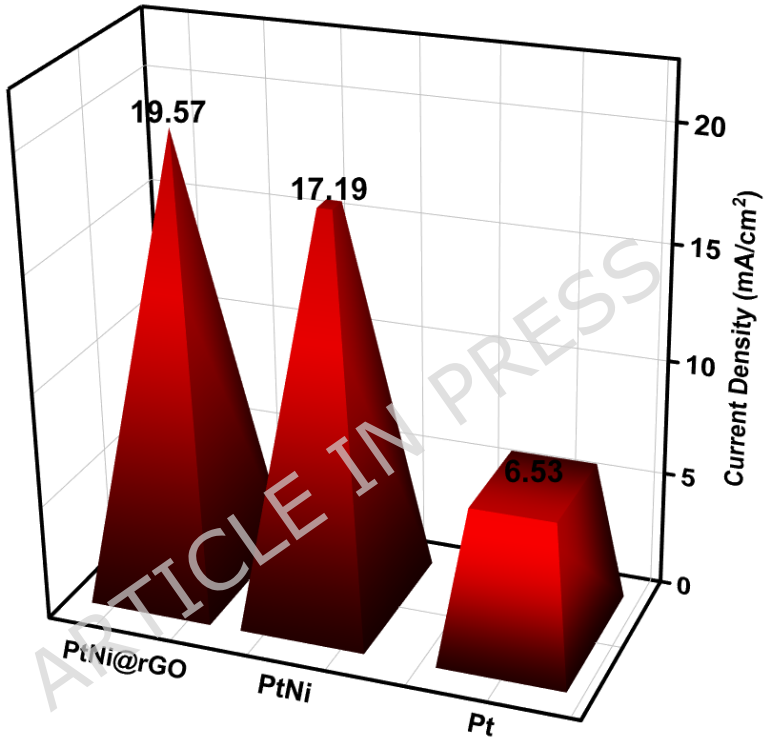


Figure 5. Comparison of current densities with CV graphs of PtNi@rGO, PtNi, and Pt nanoparticles.

Figure 6a and Figure 6b show the CV measurements of NaBH4 using the PtNi@rGO electrocatalyst at different scan rates of 50 mV/s, 100 mV/s, 125 mV/s, and 150 mV/s. Furthermore, as seen in Figure 6a, applying different scan rates results in a linear increase in current density depending on the scan rate. These results indicate that increasing scan rates (50, 100, 125, and 150 mV/s) accelerate charge transfer and increase current density. This indicates that the electrochemical reaction is kinetically accelerated. At high

ARTICLE IN PRESS

scanning speeds, the catalyst reacts more actively on the electrode surface while reducing charge transfer resistance, confirming that the reaction proceeds via a surface-controlled mechanism. This situation supports that the electrocatalyst exhibits fast electron transfer capability and high electrochemical activity. Therefore, it supports its evaluation as a highly efficient catalyst for advanced energy conversion systems [57].

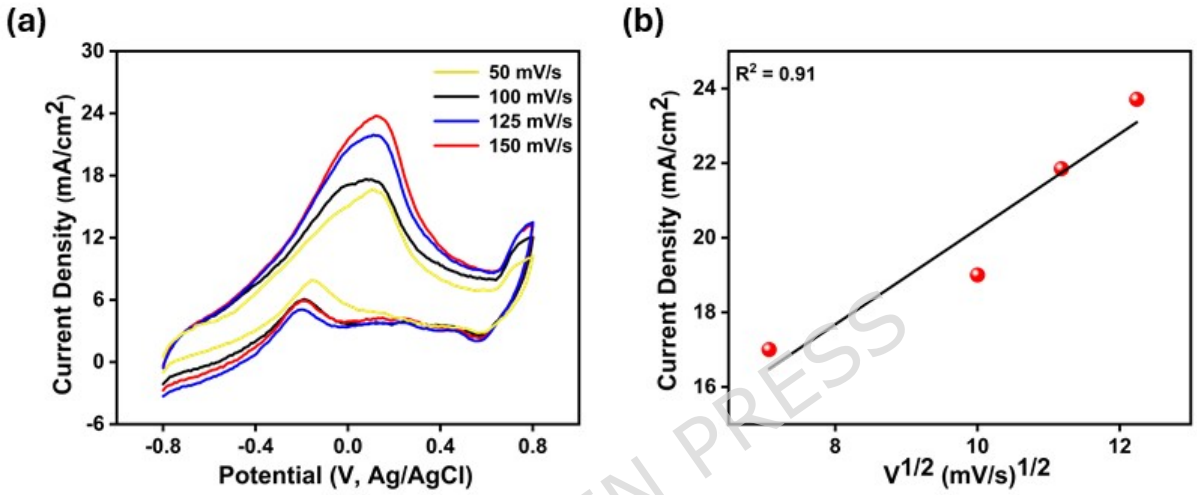


Figure 6. CV plots **(a)** and slope plot, **(b)** of PtNi@rGO at different scan rates in a 1 M NaOH solution containing 0.1 M $NaBH_4$.

The maintained catalytic activity during the CA test of the PtNi@rGO electrocatalyst is investigated using the CA method to evaluate its ability to maintain time-dependent electrochemical activity. As shown in Figure 7, CA curve initially exhibited a rapid current drop, which can be attributed to the reorganisation of the active surface and the temporary adsorption of reaction intermediates onto the surface. Following this initial phase, the system reached a relatively stable operating region and partially maintained its electrochemical activity throughout the long-term measurement. After prolonged operation, the PtNi@rGO electrode exhibited a current retention rate of approximately 15.6% compared to the initial current. Although a gradual decrease in current density was observed during the experiment, the electrode maintained its electrocatalytic activity for 4500 s. However, the

ARTICLE IN PRESS

gradual current decline observed over longer periods indicates the effects of surface passivation and side reactions occurring in the system over time. This behaviour can be explained by the Pt–Ni bimetallic centres improving the electron transfer kinetics and the highly conductive structure of rGO supporting charge transport. Considering that Pt/C and similar bimetallic systems generally exhibit significant current loss over shorter time scales in the literature, the long-term operational performance and partial current retention of the PtNi@rGO electrode demonstrate the synergistic effect of the structure. These results confirm that PtNi@rGO is a candidate for an electrocatalyst that is both active and operationally robust for borohydride oxidation [55].

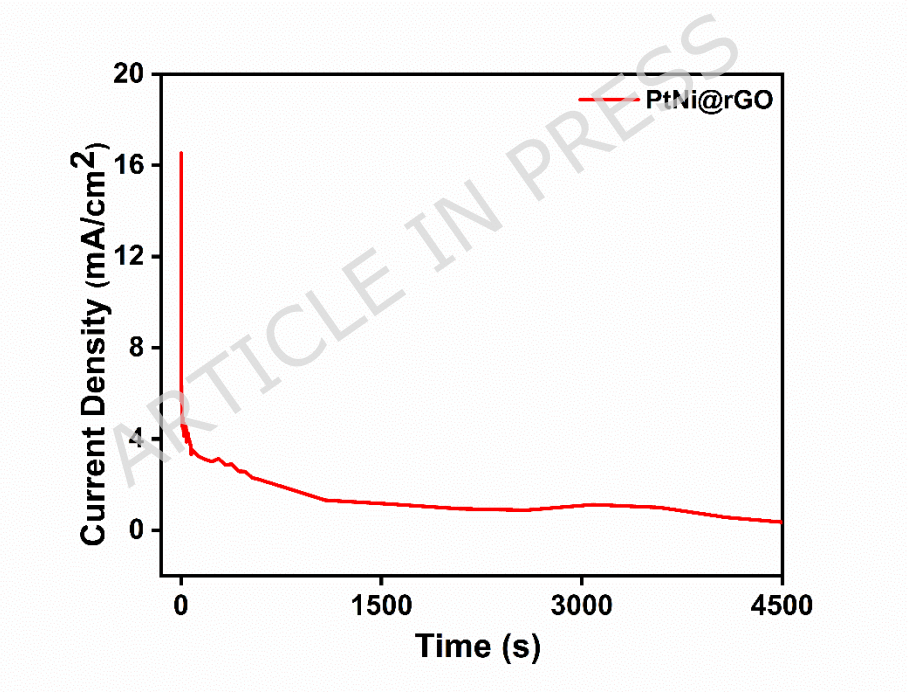


Figure 7. Maintained catalytic activity during the CA test of PtNi@rGO in a 1 M NaOH solution containing 0.1 M $NaBH_4$.

To evaluate the structural stability of the catalyst following electrochemical operation, post-reaction SEM, TEM, and FTIR analyses were performed; the results are presented in the Supplementary Information file in Figures S.1, S.2, and S.3, respectively. In the post-reaction SEM and TEM images, it was

ARTICLE IN PRESS

observed that the nanoparticles exhibited a certain degree of agglomeration on the surface and that partial changes occurred in the particle distribution (Figure S.1 and Figure S.2). However, no evidence of significant morphological collapse or phase separation indicating complete degradation of the catalytic structure was found. Upon examination of the FTIR analyses, it was observed that the pre- and post-reaction spectra generally exhibited similar characteristic bands, although limited shifts occurred at certain band positions (Figure S.3). It is thought that these changes may stem from intermediate species adsorbed on the surface during the reaction, borate derivatives, or interactions between the catalyst surface and the reaction environment. These results indicate that the current decrease observed in the chronoamperometric experiments cannot be explained solely by structural degradation; factors such as surface adsorption, active site blocking, and the accumulation of reaction intermediates may also influence catalytic performance. These findings are consistent with recent literature reporting that catalyst performance in the electrooxidation of $NaBH_4$ is closely related not only to initial activity but also to surface restructuring, adsorbed intermediate species, and catalyst-support interactions that occur during the reaction.

The comparative electrochemical data presented in Table 1 demonstrate that the developed Pt, PtNi and PtNi@rGO electrodes exhibit significantly superior performance compared to various catalysts reported in the literature for the borohydride electro-oxidation (BH_4^-) reaction. In particular, the PtNi@rGO electrode, with a maximum current density of 19.57 mA cm^{-2} and an initiation potential of 0.13 V, exhibited both the highest activity and the lowest reaction initiation energy among all the systems compared. This value indicates a significant kinetic improvement when compared to reference systems such as Pt/C (11.70 mA cm^{-2}, 0.22 V) and PtNi(3:7)/C (4.69 mA cm^{-2}). Furthermore, the achievement of a higher current density even when compared to multi-component and typically optimised catalyst systems

ARTICLE IN PRESS

such as PdAuNi/C (8.50 mA cm^{-2}) and PtNPsCu/Ti (1.60–6.10 mA cm^{-2}) systems, indicates that PtNi@rGO offers an electrode architecture that is advantageous not only compositionally but also structurally. In particular, the performance achieved in this study under lower alkalinity conditions, such as 1 M NaOH, highlights the catalyst's strong intrinsic activity, especially when considering that Pt/C and PtNi-based systems in the literature are frequently tested at higher base concentrations, such as 6 M NaOH.

Table 1. A comparison of the electrochemical performance of Pt-based and similar electrocatalysts developed for the electro-oxidation of sodium borohydride in an alkaline environment with that reported in the literatüre.

Catalyst	**Electrolyte**	**Maximum Current Density (mA cm^{-2})**	**Initial Potential (V)**	**References**
PtNPsCu/Ti	0.05 M $NaBH_4$ + 1 M NaOH	1.60–6.10	-	[58]
PdAuNi/C	0.01 M $NaBH_4$	8.50	-	[59]
PtNi(3:7)/C	0.1 M $NaBH_4$ + 6 M NaOH	4.69	-	[60]
Pt/C	0.1 M $NaBH_4$ + 6 M NaOH	11.70	-	[60]
Pt	**0.1 M $NaBH_4$ + 1 M NaOH**	**6.53**	**0.22**	**This work**
PtNi	**0.1 M $NaBH_4$ + 1 M NaOH**	**17.19**	**0.17**	**This work**
PtNi@rGO	**0.1 M $NaBH_4$ + 1 M NaOH**	**19.57**	**0.13**	**This work**

ARTICLE IN PRESS

This increase in performance indicates that the adsorption properties of Pt centres are modulated by the redistribution of electron density within the Pt–Ni bimetallic structure, leading to a faster transformation of reaction intermediates. Furthermore, the high electrical conductivity and three-dimensional network structure of the rGO support enhance the overall electrocatalytic efficiency by facilitating both a more homogeneous distribution of active sites and an acceleration of the electron transfer kinetics. This synergistic effect is particularly evident in the combination of both a low onset potential and high current density, demonstrating that it constitutes a more advantageous catalytic platform for the electro-oxidation of BH_4^- in terms of reaction kinetics and electrode efficiency compared to similar systems in the literature.

4. Conclusion

In this study, the structural properties and electrocatalytic performance of Pt, PtNi and PtNi@rGO electrodes developed for hydrogen production via the electrochemical oxidation of $NaBH_4$ were investigated in a comparative manner. FTIR, XRD, TEM and SEM-EDX analyses confirmed that the Pt–Ni bimetallic structure was successfully formed on the rGO support matrix and that the nanoparticles were homogeneously distributed. While XRD results indicated the presence of the Pt–Ni alloy phase, TEM and SEM images revealed the formation of a well-dispersed structure without significant agglomeration; EDX analyses confirmed the homogeneous distribution of the elements (Pt, Ni, C) within the composite. The maximum current densities obtained from CV measurements were determined to be 19.57 mA cm^{-2} for PtNi@rGO, 17.19 mA cm^{-2} for PtNi, and 6.53 mA cm^{-2} for Pt; the PtNi@rGO electrode exhibited approximately three times higher electrocatalytic activity compared to Pt. The reaction onset potentials were determined to be 0.13 V, 0.17 V and 0.22 V, respectively; this indicates that PtNi@rGO can initiate the reaction with a lower energy barrier and possesses improved electron transfer kinetics. The CV curves obtained at different scan rates

ARTICLE IN PRESS

demonstrated that the current density increased linearly with the scan rate for all electrodes, confirming that the process exhibits surface-controlled kinetics. The fact that the PtNi@rGO electrode exhibited a higher current response at all scan rates indicates an expanded active surface area and accelerated charge transfer. Overall, the electrochemical and structural results obtained indicate that the PtNi@rGO electrode offers both higher activity and a lower reaction initiation potential compared to Pt and PtNi references. This performance enhancement can be attributed to the synergistic effect of the Pt–Ni bimetallic interaction and the contribution of rGO's high conductivity and surface area.

Data Availability Statement

Data will be available on request.

Declaration of Competing Interest

The authors declare that they have no known competing financial interests or personal relationships that could have appeared to influence the work reported in this paper.

ARTICLE IN PRESS

Funding

The authors (E.H.) would like to thank TUBITAK 2209-A-2023/2 for the financial support.

Referenes

[1] Z. Jiang, A. Rahman Mahmud, A. Maneengam, A. A. Nassani, M. Haffar, and P. The Cong, "Non linear effect of Biomass, fossil fuels and renewable energy usage on the economic Growth: Managing sustainable development through energy sector," *Fuel*, vol. 326, p. 124943, Oct. 2022, doi: 10.1016/j.fuel.2022.124943.

[2] A. Raihan, M. Rashid, L. C. Voumik, S. Akter, and M. A. Esquivias, "The Dynamic Impacts of Economic Growth, Financial Globalization, Fossil

ARTICLE IN PRESS

Fuel, Renewable Energy, and Urbanization on Load Capacity Factor in Mexico," *Sustainability*, vol. 15, no. 18, p. 13462, Sep. 2023, doi: 10.3390/su151813462.

[3] S. Berdysheva and S. Ikonnikova, "The Energy Transition and Shifts in Fossil Fuel Use: The Study of International Energy Trade and Energy Security Dynamics," *Energies*, vol. 14, no. 17, p. 5396, Aug. 2021, doi: 10.3390/en14175396.

[4] P. Nikolaidis and A. Poullikkas, "A comparative overview of hydrogen production processes," *Renew. Sustain. Energy Rev.*, vol. 67, pp. 597–611, Jan. 2017, doi: 10.1016/J.RSER.2016.09.044.

[5] A. G. Olabi and M. A. Abdelkareem, "Renewable energy and climate change," *Renew. Sustain. Energy Rev.*, vol. 158, p. 112111, Apr. 2022, doi: 10.1016/j.rser.2022.112111.

[6] H. N. Abdelhamid, "A review on hydrogen generation from the hydrolysis of sodium borohydride," *Int. J. Hydrogen Energy*, vol. 46, no. 1, pp. 726–765, 2021, doi: 10.1016/j.ijhydene.2020.09.186.

[7] V. G. Minkina, S. I. Shabunya, V. I. Kalinin, and V. V. Martynenko, "Hydrogen generation from hydrolysis of concentrated NaBH4 solutions under adiabatic conditions," *Int. J. Hydrogen Energy*, vol. 47, no. 51, pp. 21772–21781, Jun. 2022, doi: 10.1016/j.ijhydene.2022.05.006.

[8] M. Kabir *et al.*, "Climate change due to increasing concentration of carbon dioxide and its impacts on environment in 21st century; a mini review," *J. King Saud Univ. - Sci.*, vol. 35, no. 5, p. 102693, Jul. 2023, doi: 10.1016/j.jksus.2023.102693.

[9] K. R. Abbasi, M. Shahbaz, J. Zhang, M. Irfan, and R. Alvarado, "Analyze the environmental sustainability factors of China: The role of fossil fuel energy and renewable energy," *Renew. Energy*, vol. 187, pp. 390–402,

ARTICLE IN PRESS

Mar. 2022, doi: 10.1016/j.renene.2022.01.066.

[10] S. Valizadeh *et al.*, “Valorization of biomass through gasification for green hydrogen generation: A comprehensive review,” *Bioresour. Technol.*, vol. 365, p. 128143, Dec. 2022, doi: 10.1016/j.biortech.2022.128143.

[11] A. K. Sarker, A. K. Azad, M. G. Rasul, and A. T. Doppalapudi, “Prospect of Green Hydrogen Generation from Hybrid Renewable Energy Sources: A Review,” *Energies*, vol. 16, no. 3, p. 1556, Feb. 2023, doi: 10.3390/en16031556.

[12] R. Darabi *et al.*, “Synthesis, characterization, and enhanced hydrogen generation from NaBH4 methanolysis of highly dispersed bimetallic PdNi nanoparticles supported on Vulcan carbon,” *Mol. Catal.*, vol. 547, p. 113245, Aug. 2023, doi: 10.1016/j.mcat.2023.113245.

[13] Y. Wu *et al.*, “Hydrogen generation from methanolysis of sodium borohydride using waste coffee oil modified zinc oxide nanoparticles and their photocatalytic activities,” *Int. J. Hydrogen Energy*, vol. 48, no. 17, pp. 6613–6623, Feb. 2023, doi: 10.1016/j.ijhydene.2022.04.177.

[14] A. Aygun *et al.*, “Highly active PdPt bimetallic nanoparticles synthesized by one-step bioreduction method: Characterizations, anticancer, antibacterial activities and evaluation of their catalytic effect for hydrogen generation,” *Int. J. Hydrogen Energy*, vol. 48, no. 17, pp. 6666–6679, Feb. 2023, doi: 10.1016/j.ijhydene.2021.12.144.

[15] J. Song, R. Li, and H. Dong, “Controllable hydrogen production from NaBH4 hydrolysis promoted by acetic acid,” *Int. J. Hydrogen Energy*, vol. 48, no. 22, pp. 8093–8100, Mar. 2023, doi: 10.1016/j.ijhydene.2022.11.204.

[16] F. Xu *et al.*, “A review of hydrogen production kinetics from the hydrolysis of NaBH4 solution catalyzed by Co-based catalysts,” *Int. J.*

ARTICLE IN PRESS

Hydrogen Energy, vol. 50, pp. 827–844, Jan. 2024, doi: 10.1016/j.ijhydene.2023.08.142.

[17] M. Dragan, “Hydrogen Storage in Complex Metal Hydrides NaBH4: Hydrolysis Reaction and Experimental Strategies,” *Catalysts*, vol. 12, no. 4, p. 356, Mar. 2022, doi: 10.3390/catal12040356.

[18] F. Ameen *et al.*, “Photocatalytic investigation of textile dyes and E. coli bacteria from wastewater using Fe3O4@MnO2 heterojunction and investigation for hydrogen generation on NaBH4 hydrolysis,” *Environ. Res.*, vol. 220, p. 115231, Mar. 2023, doi: 10.1016/j.envres.2023.115231.

[19] A. Soltani *et al.*, “ZnSnO3 - SnO2 nanocomposite as a catalyst for efficient hydrogen production through sodium borohydride methanolysis,” *Int. J. Hydrogen Energy*, vol. 67, pp. 429–437, May 2024, doi: 10.1016/j.ijhydene.2024.04.208.

[20] J. Lin *et al.*, “Phyto-mediated synthesis of nanoparticles and their applications on hydrogen generation on NaBH4, biological activities and photodegradation on azo dyes: Development of machine learning model,” *Food Chem. Toxicol.*, vol. 163, p. 112972, May 2022, doi: 10.1016/j.fct.2022.112972.

[21] F. Karimi *et al.*, “Facile bio-fabrication of ZnO@AC nanoparticles from chitosan: Characterization, hydrogen generation, and photocatalytic properties,” *Environ. Res.*, vol. 216, p. 114668, Jan. 2023, doi: 10.1016/j.envres.2022.114668.

[22] Y. Zhu *et al.*, “Closing the Loop for Hydrogen Storage: Facile Regeneration of NaBH 4 from its Hydrolytic Product,” *Angew. Chemie*, vol. 132, no. 22, pp. 8701–8707, May 2020, doi: 10.1002/ange.201915988.

[23] K. Gokkus, A. Ozbal, M. Gür, S. A. Akalin, and V. Bütün,

ARTICLE IN PRESS

"Hyperbranched novel functional polymeric catalysts offering new approaches in hydrogen production via NaBH4 methanolysis," *Int. J. Hydrogen Energy*, vol. 98, pp. 106–126, Jan. 2025, doi: 10.1016/j.ijhydene.2024.12.059.

[24] Y. Wu *et al.*, "Synthesis of novel activated carbon-supported trimetallic Pt–Ru–Ni nanoparticles using wood chips as efficient catalysts for the hydrogen generation from NaBH4 and enhanced photodegradation on methylene blue," *Int. J. Hydrogen Energy*, vol. 48, no. 55, pp. 21055–21065, Jun. 2023, doi: 10.1016/j.ijhydene.2022.07.152.

[25] Ü. Ecer, A. Zengin, and T. Şahan, "Hydrogen generation from NaBH4 hydrolysis catalyzed by cobalt (0)-Deposited cross-linked polymer brushes: Optimization with an experimental design approach," *Int. J. Hydrogen Energy*, vol. 48, no. 34, pp. 12814–12825, Apr. 2023, doi: 10.1016/j.ijhydene.2022.12.224.

[26] I. Belkoufa *et al.*, "Improved thermodynamic properties of (Sc, V, Ti, Fe, Mn, Co, and Ni) doped NaBH4 for hydrogen storage: First-principal calculation," *Int. J. Hydrogen Energy*, vol. 68, pp. 481–490, May 2024, doi: 10.1016/j.ijhydene.2024.04.155.

[27] A. Kytsya *et al.*, "Bimetallic Ni-Co nanoparticles as an efficient catalyst of hydrogen generation via hydrolysis of NaBH4," *J. Alloys Compd.*, vol. 908, p. 164484, Jul. 2022, doi: 10.1016/j.jallcom.2022.164484.

[28] R. Bayat, E. Halvaci, T. Kozak, M. Bekmezci, and F. Sen, "Electrocatalytic performance of Shape-Controlled synthesized PdNi-rGO nano Cube on sodium borohydride and methanol electrooxidation," *Fuel*, vol. 366, p. 131248, Jun. 2024, doi: 10.1016/j.fuel.2024.131248.

[29] Z. Daşdelen, Y. Yıldız, S. Eriş, and F. Şen, "Enhanced electrocatalytic activity and durability of Pt nanoparticles decorated on GO-PVP

ARTICLE IN PRESS

hybride material for methanol oxidation reaction," *Appl. Catal. B Environ.*, vol. 219, pp. 511–516, Dec. 2017, doi: 10.1016/j.apcatb.2017.08.014.

[30] A. Ponrouch and M. R. Palacín, "On the impact of the slurry mixing procedure in the electrochemical performance of composite electrodes for Li-ion batteries: A case study for mesocarbon microbeads (MCMB) graphite and Co3O4," *J. Power Sources*, vol. 196, no. 22, pp. 9682–9688, Nov. 2011, doi: 10.1016/j.jpowsour.2011.07.045.

[31] H. Göksu, K. Cellat, and F. Şen, "Single-Walled Carbon Nanotube Supported PtNi Nanoparticles (PtNi@SWCNT) Catalyzed Oxidation of Benzyl Alcohols to the Benzaldehyde Derivatives in Oxygen Atmosphere," *Sci. Rep.*, vol. 10, no. 1, p. 9656, Jun. 2020, doi: 10.1038/s41598-020-66492-x.

[32] H. Burhan, H. Ay, E. Kuyuldar, and F. Sen, "Monodisperse Pt-Co/GO anodes with varying Pt: Co ratios as highly active and stable electrocatalysts for methanol electrooxidation reaction," *Sci. Rep.*, vol. 10, no. 1, p. 6114, Apr. 2020, doi: 10.1038/s41598-020-63247-6.

[33] S. Eris, Z. Daşdelen, and F. Sen, "Investigation of electrocatalytic activity and stability of Pt@f-VC catalyst prepared by in-situ synthesis for Methanol electrooxidation," *Int. J. Hydrogen Energy*, vol. 43, no. 1, pp. 385–390, 2018, doi: https://doi.org/10.1016/j.ijhydene.2017.11.063.

[34] S. Eris, Z. Daşdelen, and F. Sen, "Enhanced electrocatalytic activity and stability of monodisperse Pt nanocomposites for direct methanol fuel cells," *J. Colloid Interface Sci.*, vol. 513, pp. 767–773, Mar. 2018, doi: 10.1016/j.jcis.2017.11.085.

[35] N. I. Zaaba, K. L. Foo, U. Hashim, S. J. Tan, W.-W. Liu, and C. H. Voon, "Synthesis of graphene oxide using modified hummers method: solvent influence," *Procedia Eng.*, vol. 184, pp. 469–477, Jan. 2017, doi:

ARTICLE IN PRESS

10.1016/j.proeng.2017.04.118.

[36] R. Darabi *et al.*, “Simultaneous determination of ascorbic acid, dopamine, and uric acid with a highly selective and sensitive reduced graphene oxide/polypyrrole-platinum nanocomposite modified electrochemical sensor,” *Electrochim. Acta*, vol. 457, p. 142402, Jul. 2023, doi: 10.1016/j.electacta.2023.142402.

[37] S. N. Alam, N. Sharma, and L. Kumar, “Synthesis of Graphene Oxide (GO) by Modified Hummers Method and Its Thermal Reduction to Obtain Reduced Graphene Oxide (rGO)*,” *Graphene*, vol. 06, no. 01, pp. 1–18, Jan. 2017, doi: 10.4236/graphene.2017.61001.

[38] S. Kaya, A. Caglar, C. Saka, and H. Kivrak, “Methanolysis and electrooxidation of sodium borohydride on CNT supported Pd and Au bimetallic catalysts,” *J. Electroanal. Chem.*, vol. 956, p. 118110, Mar. 2024, doi: 10.1016/j.jelechem.2024.118110.

[39] M. Brycht *et al.*, “Synthesis and characterization of the thermally reduced graphene oxide in argon atmosphere, and its application to construct graphene paste electrode as a naptalam electrochemical sensor,” *Anal. Chim. Acta*, vol. 1035, pp. 22–31, Dec. 2018, doi: 10.1016/j.aca.2018.06.057.

[40] Y. Veera Manohara Reddy *et al.*, “Ultrafine Pt–Ni bimetallic nanoparticles anchored on reduced graphene oxide nanocomposites for boosting electrochemical detection of dopamine in biological samples,” *New J. Chem.*, vol. 42, no. 20, pp. 16891–16901, 2018, doi: 10.1039/C8NJ03894E.

[41] C. Rodríguez-Proenza *et al.*, “Atomic Surface Segregation and Structural Characterization of PdPt Bimetallic Nanoparticles,” *Materials (Basel).*, vol. 11, no. 10, p. 1882, Oct. 2018, doi: 10.3390/ma11101882.

ARTICLE IN PRESS

ARTICLE IN PRESS

[42] W. Ji, W. Qi, S. Tang, H. Peng, and S. Li, “Hydrothermal Synthesis of Ultrasmall Pt Nanoparticles as Highly Active Electrocatalysts for Methanol Oxidation,” *Nanomaterials*, vol. 5, no. 4, pp. 2203–2211, Dec. 2015, doi: 10.3390/nano5042203.

[43] P. K. Sahoo, B. Panigrahy, and D. Bahadur, “Facile synthesis of reduced graphene oxide/Pt–Ni nanocatalysts: their magnetic and catalytic properties,” *RSC Adv.*, vol. 4, no. 89, pp. 48563–48571, 2014, doi: 10.1039/C4RA07686A.

[44] K. Kannan, D. Chanda, M. M. Meshesha, and B. Yang, “Impressive efficiency of zinc oxide-manganese oxide/MAX composite in two-electrode system for photovoltaic-electrolyzer water splitting,” *Colloids Surfaces A Physicochem. Eng. Asp.*, vol. 689, p. 133599, May 2024, doi: 10.1016/j.colsurfa.2024.133599.

[45] K. Kannan *et al.*, “Hydrothermally synthesized mixed metal oxide nanocomposites for electrochemical water splitting and photocatalytic hydrogen production,” *Int. J. Hydrogen Energy*, vol. 48, no. 93, pp. 36412–36426, Dec. 2023, doi: 10.1016/j.ijhydene.2023.06.042.

[46] K. Kannan *et al.*, “Investigation of the Electrochemical Behavior of CuO-NiO-Co3O4 Nanocomposites for Enhanced Supercapacitor Applications,” *Materials (Basel).*, vol. 17, no. 16, p. 3976, Aug. 2024, doi: 10.3390/ma17163976.

[47] A. M. Huízar-Félix *et al.*, “Magnetic properties of thermally reduced graphene oxide decorated with PtNi nanoparticles,” *J. Alloys Compd.*, vol. 678, pp. 541–548, Sep. 2016, doi: 10.1016/j.jallcom.2016.03.261.

[48] T. Niu, X. Deng, R. Wang, and C. Zhou, “GO-PtNi hybrid nanoenzyme mimics for the colorimetric detection of hydrogen peroxide,” *Mater. Today Chem.*, vol. 7, pp. 35–39, Mar. 2018, doi: 10.1016/j.mtchem.2017.10.003.

ARTICLE IN PRESS

[49] R. Wei *et al.*, “Self-assembled PtNi layered metallene nanobowls for pH-universal electrocatalytic hydrogen evolution,” *J. Colloid Interface Sci.*, vol. 667, pp. 175–183, Aug. 2024, doi: 10.1016/j.jcis.2024.04.060.

[50] C. Ouyang, D. Xun, and G. Jian, “N-Doped and Sulfonated Reduced Graphene Oxide Supported PtNi Nanoparticles as Highly Efficient Electrocatalysts for Oxygen Reduction Reaction,” *Coatings*, vol. 12, no. 8, p. 1049, Jul. 2022, doi: 10.3390/coatings12081049.

[51] F.-G. He, J.-Y. Yin, G. Sharma, A. Kumar, F. J. Stadler, and B. Du, “Facile Fabrication of Hierarchical rGO/PANI@PtNi Nanocomposite via Microwave-Assisted Treatment for Non-Enzymatic Detection of Hydrogen Peroxide,” *Nanomaterials*, vol. 9, no. 8, p. 1109, Aug. 2019, doi: 10.3390/nano9081109.

[52] S. Ghasemi, S. R. Hosseini, and Z. Kazemi, “Electrochemical deposition of Pt-Ni on reduced graphene oxide as counter electrode material for dye-sensitized solar cell,” *J. Photochem. Photobiol. A Chem.*, vol. 348, pp. 263–268, Nov. 2017, doi: 10.1016/j.jphotochem.2017.08.057.

[53] A. Caglar, T. A. Hansu, O. Sahin, and H. Kivrak, “The characterization and sodium borohydride electrooxidation of novel carbon nanotube supported copromoted Pd as anode catalyst for fuel cell,” *Energy Storage*, vol. 4, no. 2, Apr. 2022, doi: 10.1002/est2.301.

[54] M. Guo, Y. Cheng, Y. Yu, and J. Hu, “Ni-Co nanoparticles immobilized on a 3D Ni foam template as a highly efficient catalyst for borohydride electrooxidation in alkaline medium,” *Appl. Surf. Sci.*, vol. 416, pp. 439–445, Sep. 2017, doi: 10.1016/j.apsusc.2017.04.193.

[55] M. G. Hosseini, N. Rashidi, R. Mahmoodi, and M. Omer, “Preparation of Pt/G and PtNi/G nanocatalysts with high electrocatalytic activity for borohydride oxidation and investigation of different operation condition on the performance of direct borohydride-hydrogen peroxide

ARTICLE IN PRESS

fuel cell," *Mater. Chem. Phys.*, vol. 208, pp. 207–219, Apr. 2018, doi: 10.1016/j.matchemphys.2018.01.018.

[56] B. Molina Concha and M. Chatenet, "Direct oxidation of sodium borohydride on Pt, Ag and alloyed Pt–Ag electrodes in basic media. Part I: Bulk electrodes," *Electrochim. Acta*, vol. 54, no. 26, pp. 6119–6129, Nov. 2009, doi: 10.1016/j.electacta.2009.05.027.

[57] S. Kottarathil *et al.*, "Selective Borohydride Oxidation Reactions of Zeolitic Imidazolate Framework-Derived Bimetallic Carbon Alloy Electrocatalysts for Alkaline Fuel Cell Applications," *ACS Appl. Energy Mater.*, vol. 5, no. 10, pp. 12571–12582, Oct. 2022, doi: 10.1021/acsaem.2c02133.

[58] A. Balčiūnaitė *et al.*, "Platinum Nanoparticles Modified Copper/Titanium Electrodes as Electrocatalysts for Borohydride Oxidation," *Materials (Basel).*, vol. 14, no. 24, p. 7663, Dec. 2021, doi: 10.3390/ma14247663.

[59] A. ElSheikh *et al.*, "Carbon-Supported Trimetallic Catalysts (PdAuNi/C) for Borohydride Oxidation Reaction," *Nanomaterials*, vol. 11, no. 6, p. 1441, May 2021, doi: 10.3390/nano11061441.

[60] G. Wang, Y. Gao, Z. Wang, C. Du, J. Wang, and G. Yin, "Investigation of PtNi/C anode electrocatalysts for direct borohydride fuel cell," *J. Power Sources*, vol. 195, no. 1, pp. 185–189, Jan. 2010, doi: 10.1016/j.jpowsour.2009.06.080.

ARTICLE IN PRESS